International Journal of GEOMATE, April, 2026 Vol.30, Issue 140, pp.115-123
ISSN: 2186-2982 (P), 2186-2990 (O), Japan, DOI: https://doi.org/10.21660/2026.140.g15286
Geotechnique, Construction Materials and Environment

EXPERIMENTAL GLOBAL–LOCAL NONLINEAR RESPONSE OF FOUNDATION–SUPERSTRUCTURE UNDER SEISMIC LOADING

*Zain Bin Mazhar[1], Faruk Md Omar[2] and Masato Saitoh[3]

[1,2,3]Graduate School of Science and Engineering, Saitama University, Japan

*Corresponding Author, Received: 30 May 2025, Revised: 16 Jan. 2026, Accepted: 17 Jan. 2026

ABSTRACT: Nowadays, as the expected earthquake motions become significantly larger, the ultimate seismic performance of large foundations, such as the caisson foundation, needs to be investigated. This study examines the seismic response of a caisson foundation connected to a superstructure modeled as a single-degree-of-freedom system. This study focuses on the inertial effects and nonlinear soil-structure interaction of the entire system under four simulated earthquake records with varying amplitudes. In particular, attention is given to soil nonlinearity (yielding and failure) and interface nonlinearity between the soil and the caisson surface in contact with the soil. These factors may influence the inertial system of soil-caisson-superstructure in terms of its resonant period and damping characteristics. To investigate the seismic response under 1g condition, a 1/40 scaled model of a caisson foundation and superstructure is used, with a diameter and height of 350 mm and 500 mm, respectively. The effects of soil and interface nonlinearities on the stiffness and damping of the superstructure interacting with the soil are evaluated using transfer functions, phase differences, pressure responses, and mean shear strain. Furthermore, the study examines the potential shift in dominant vibration modes, such as increased rocking motion of the caisson foundation with larger loading amplitudes. This research highlights the significance of soil and interface nonlinearities on the inertial behaviour of the soil-caisson-superstructure system under stimulated earthquake ground motions.

Keywords: Soil structure interaction, Caisson foundation, Non-linear analysis, SDOF Superstructure, Seismic motion

1. INTRODUCTION

Dynamic soil-structure interaction is an important factor that governs the seismic response of foundation systems, as it controls the mutual dynamic behavior of the foundation, the soil and the attached superstructure [1]. With the increasing strength of predicted earthquake ground movements, it has become crucial to properly evaluate the seismic performance of large foundations connected to the superstructures, particularly the caisson foundations. Amid high-amplitude earthquakes, the soil may undergo yielding both globally and locally. The presence of global and local nonlinearities in the soil medium can lead to complex soil-structure interaction behaviour. To have a better understanding of these mechanisms, it is imperative to delve deeper into the key parameters, such as strain-dependent soil properties related to global nonlinearities and near-field pressure response associated with local nonlinearities.

Such effects are often overlooked in the design practice, where the superstructure is assumed to be fixed at the base; however, this assumption doesn't accurately reflect the real behaviour [2]. The analysis of seismic response for soil-caisson foundation is therefore of utmost importance, as caisson foundations support structures like highway bridges, which are prone to failure under strong seismic activity. Several such structures experienced severe damage during the devastating earthquake event in Kobe, Japan, on 17 January 1995 [3]. This large-magnitude earthquake prompted significant revisions to seismic design codes, as the observed failures highlighted the need of accurate evaluation of inertial force transmission between soil, foundation, and superstructure [4]. The interaction of these inertial forces results in their propagation through the soil-foundation-structure system, leading to the elongation of the structure's natural period during seismic activity. The propagation of inertial forces and elongation of natural period can produce devastating effects on the soil-caisson system under the influence of high-amplitude seismic waves. Hence, the overall safety of the soil-foundation-structure is strongly influenced by these inertial forces [5].

Monitoring the transfer function of the soil-foundation-structure provides a valuable insight into the changes in stiffness and damping due to nonlinearities. This study investigates the variations in the amplification ratio and the phase difference owing to global and local nonlinearities. The global change in shear strain alters the soil's shear modulus of the soil, which ultimately affects the damping characteristics of the soil. As seismic waves propagate, the strain-dependent properties of soil, like shear modulus and stiffness of the material, undergo significant changes, impacting the dynamic response of the entire structure [6, 7]. Additionally, this study

further explores the local failures and demonstrates that the variations in the transfer function are closely linked with local nonlinearities as described in a study done by [8, 9]. Analyzing near-field pressure response of the soil-foundation-structure for such local failures can provide insight into pronounced reduction in the amplitude of the transfer function with the increase of seismic amplitude [10, 11].

While most researchers have concentrated on the inertial effects of superstructure and pile foundation, assuming linear soil behaviour, often overlooking the nonlinear soil behaviour and its interaction with supporting structures, this study is intended to address this gap. It closely monitors the behaviour of the caisson foundation coupled with the single degree of freedom (SDOF) superstructure under the influence of four different earthquake records. The main objectives of this research are: 1) To investigate the response of caisson foundations under seismic motions with large amplitudes, aiming to capture critical system behaviors and conditions that lead to severe damage, 2) To study the effects of amplitude on the amplification ratio and the natural period elongation, 3) To examine the mechanics of soil-caisson-structure interaction, such as pressure response for local nonlinearities and mean shear strain for both global and local nonlinearities.

2. RESEARCH SIGNIFICANCE

This research highlights the importance of bridging gaps in understanding the critical response of soil-caisson-superstructure interaction under real earthquakes. Caisson foundations are used in infrastructure projects like bridges and wind turbines, where they play a crucial role in transferring dynamic loads from the soil to the super structure. The nonlinear behaviour of the surrounding soil presents a major challenge for researchers and engineers in predicting the dynamic response of such massive foundations. Under high amplitude loading, the soil-structure-interaction becomes increasingly complex, demonstrating a response that is remarkably different from the linear behaviour of soil.

By considering the nonlinear nature of soil carefully, this study analyzes the elongation of the natural period and changes in the amplification ratio against seismic records of high amplitudes. These parameters have a significant impact on the dynamic response of the overall system, and any changes in them can alter the performance of both the foundation and the superstructure. The findings of this study provide valuable insight into the dynamic characteristics of the soil-caisson-superstructure system, which can be beneficial in improving overall resilience. It further explores how inertial effects can produce global and local nonlinearities around the caisson foundation, enhancing the understanding of global changes in soil material and local interface failures between soil and the foundation. These failures may result from the inertial effects of seismic activity itself or from the superstructure. Ultimately, this research work will contribute to the safer design of the infrastructure subjected to strong seismic activity.

3. MODEL TEST

Scaling rules are essential to accurately build a relationship between the real model and its prototype. Scaling rules are essential to accurately build a relationship between the real model and its prototype for experimental studies in small-scale environments. The experimental setup of this study is scaled as per the scaling rule developed by [12].

Table 1. Model to prototype scaling parameters

	Quantity	Law of similitude	Factor of similitude	Value of every quantity		
				Prototype	Target value	Attained value
Subsurface Layer	Depth of Layer (m)	λ	0.03	17	0.4	0.4
	Density (t/m^3)	η	0.8	1.8	1.4	1.6
	Natural Frequency (Hz)	$\lambda^{-0.25}\eta^{-0.75}$	17	2.2	37.3	38.1
	Shear Velocity (m/s)	$\lambda^{-0.25}\eta^{-0.25}$	0.4	150	64	65.5
Bedrock Layer	Depth of layer (m)	λ	0.03	8	0.2	0.2
	Density (t/m^3)	η	0.8	2.0	1.5	1.6
	Shear Velocity (m/s)	$\lambda^{-0.25}\eta^{-0.25}$	0.4	400	171	142
Foundation	Length (m)	λ	0.03	17	0.4	0.4
	Diameter (m)	λ	0.03	14	0.4	0.4
	Thickness (m)	λ	0.03	0.8	0.02	0.02
	Yung's Modulus (KN/m^3)	$\lambda^{0.5}\eta^{0.5}$	0.1	2.5×10^7	3.5×10^6	3.0×10^6
	Moment of Inertia (m^4)	λ^4	4.1×10^{-7}	700.5	2.9×10^{-4}	2.9×10^{-4}

The frequency ratio of the model to the prototype is evaluated as shown below, considering both geometry and density conditions.

$$\frac{\omega_m}{\omega_p} = \lambda^{-0.25}\eta^{-0.75} \quad (1)$$

In the equation shown above, λ represents the geometrical properties, whereas η represents the material density characteristic. As per the same scaling law, the model-to-prototype strain ratio is:

$$\frac{\gamma_m}{\gamma_p} = \lambda^{0.5}\eta^{0.5} \quad (2)$$

The rules and factors as per the law, for both the prototype and the model, are compiled in Table 1

4. EXPERIMENTAL SETUP

Fig. 1 shows the experimental configuration of this study.

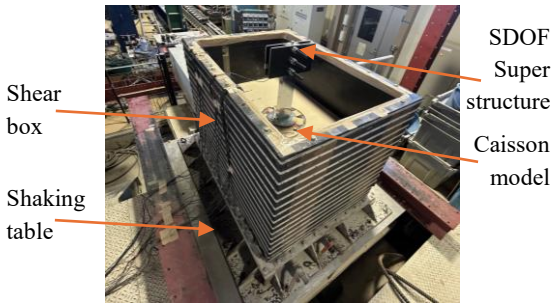

Fig. 1 Experimental setup in the laboratory

The caisson foundation in this experiment is placed within a shear box with inner dimensions of 1200 mm, 800 mm, and 1000 mm for length, width, and depth, respectively.

These dimensions are similar to those used by [13-16]. The shear box is bolted on the top of a 1.8 m^2 unidirectional shaking table.

4.1. Soil material

The shear box is filled with Gifu sand arranged in two different layers: a moist bottom layer with 8% moisture content providing firm support for the base of the foundation and a dry top layer with a specific gravity of 2.64.

The layer at the base is compacted with a heavy weight dropped under the influence of gravity, whereas the top layer is compacted by providing base vibration of 6m/s^2 and 40 Hz frequency through a shaking table to achieve the target density of 1.4 t/m^3.

4.2. Foundation model and instrumentation

At the center of the shear box, a model of a caisson foundation with a 350 mm diameter, 450 mm height, and 20 mm wall thickness is placed. The hollow cylindrical caisson is meticulously filled with dry Gifu sand. The mass and volume are carefully adjusted to achieve the desired scaled parameters. A Single degree of freedom (SDOF) superstructure, measuring 500 mm in height and carrying 56.8 kg of mass at its head, is attached to the head of the caisson foundation, with a natural frequency of 23.7 Hz.

The instrumentation layout shown in Fig. 2 consists of multiple accelerometers and pressure meters. Eight pressure transducers (CH8–CH15) are attached to the body of the caisson foundation. In addition, eleven accelerometers (CH2–CH7, CH16–CH19) are used: one at the shaking table, six within the sand, three at the head of the foundation, and one on the head of superstructure.

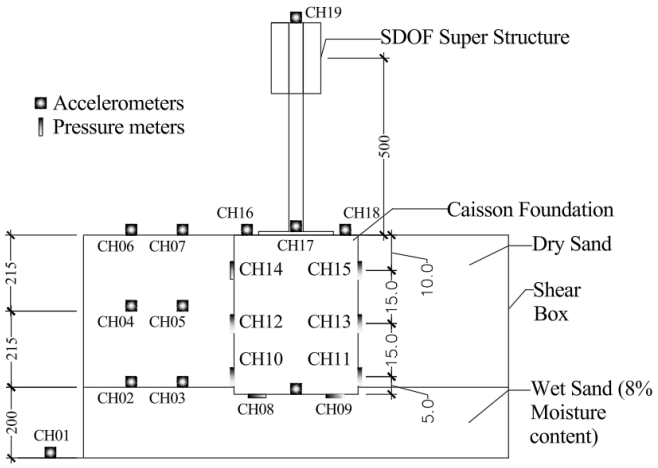

Fig. 2 Schematic representation of the test setup

4.3. Loading conditions

Table 2. Input Ground excitation measured at CH7

Input Case	El-Centro m/s^2	Kobe m/s^2	Ojiya m/s^2	White noise m/s^2
S1	0.728	1.153	1.365	1.608
S2	1.972	3.124	3.124	2.730
L1	4.398	6.522	7.037	11.345
L2	8.372	13.256	11.800	15.167
L3	11.557	12.892	12.649	18.261
L4	10.981	11.800	13.225	16.774
L5	14.075	16.048	15.409	24.294

The experiment was conducted using four earthquake records: the 1940 El-Centro (NS), the 1995 JMA Kobe (NS), the 2004 K-Net Ojiya (EW), and White noise. All records were scaled to simulate realistic earthquake conditions. Seven distinct input motions were applied through a shaking table, transmitting the excitation to the ground. The resulting excitation amplitudes recorded at the ground surface (CH07) are listed in Table 2, hereafter referred as S1, S2, L1, L2, L3, L4, and L5. For each case, the relative displacement, defined as the distance covered by sand particles at the ground surface relative to the base due to deformation, was measured. Additionally, the mean shear strain that describes the shear strain distribution along the depth of the sand was also measured to support the study's objective.

5. DATA PROCESSING

The experimental data were recorded in the form of time histories for both acceleration and pressure. Fourier Transformation (FFT) was later used to convert the time domain data to the frequency domain, followed by the calculation of the transfer function using the cross spectrum and power-spectrum from multiple response waveforms that were recorded under the same conditions. The noise was then removed using an averaging process applied to the spectra.

Finally, the amplification ratio curves were prepared for the superstructure and the caisson head with respect to the ground surface, concerning the input motion. To measure near-field pressure from time history, the peak pressure for all earthquake records was recorded for their respective amplitudes.

6. RESULTS AND DISCUSSION

6.1. Relative displacement and mean shear strain

Fig. 3 shows the mean shear strain (y-axis) with loading amplitude (x-axis) for all earthquake records. The graph demonstrates the results from the top to the bottom of the sand. For lower amplitudes, the minimum shear strain remains minimal but increases drastically above 10 m/s^2 because the soil softens upon transition from linear to nonlinear state. This high-strain behaviour results in high energy dissipation due to particle rearrangement.

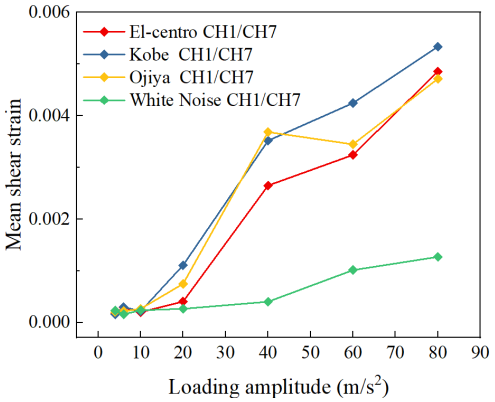

Fig. 3 Mean shear strain from the base to the ground

The corresponding average relative displacement and mean shear strain values are shown in Table 3.

Table 3. Relative displacement and mean shear strain

Case	Relative displacement (m)	Mean shear strain (%)
S1	0.0001953	0.031
S2	0.0002443	0.039
L1	0.000232	0.037
L2	0.0006348	0.101
L3	0.0025653	0.407
L4	0.0029888	0.474
L5	0.004046	0.642

6.2. Superstructure head

6.2.1. Horizontal transfer function

Fig. 4 illustrates the amplitude of the horizontal transfer function (amplification ratio) at the head of the superstructure with respect to the ground surface, subjected to the earthquake records of increasing amplitude. At amplitudes lower than L1, the system depicts the linear state. Case L1 can be considered as the transitional amplitude, as indicated by Table 3, which shows smaller mean shear strain values for S1 and S2, with a sudden rise above L1.

As the soil yields with the increase in mean shear strain, the shear modulus decreases rapidly. This reduction intensifies with the increase in shear strain. This phenomenon reflects global nonlinearity, where the soil-structure system exhibits a nonlinear response. The loss of stiffness and strength of the soil

material leads to prominent energy dissipation. resulting in increased damping, consequently, a decrease in the amplification ratio. Besides this, for higher amplitudes, local nonlinearity is predicted as the soil undergoes large amounts of strain for localized areas near the foundation.

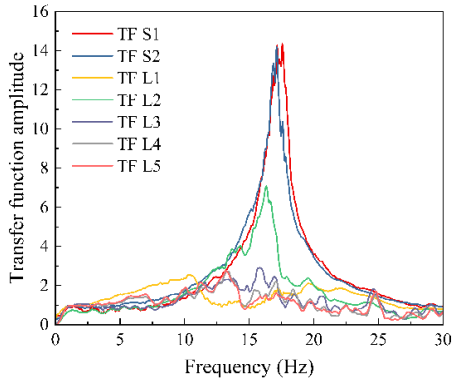

Fig. 4 Transfer function at the head of the super structure with respect to the ground surface

Before yielding, the small-strain behaviour dominates, where the shear modulus remains relatively constant. After yielding, the soil transitions to a plastic deformation state, resulting in a significant reduction in the overall stiffness, closely linked to the decrease in the elastic modulus of the soil. This represents global nonlinearity in the soil, where the entire soil system undergoes significant changes. Furthermore, at the higher strain levels, phenomena such as dropping of shear modulus to a minimum level and rising of the damping to its maximum level significantly influences the soil-structure interaction. Here, the separation between the soil and the foundation can also be predicted, indicating local yielding.

As a result, the peak of the amplification ratio decreases with the increase in loading amplitude, eventually becoming almost flat for the state of soil where a large amount of energy has been dissipated due to a significant increase in damping, accompanied by a massive reduction in strength and stiffness. Additionally, for higher amplitudes, a backwards shift in the peak of the graph towards lower frequencies can also be seen. This reduction in the natural frequency of the system is due to the softening of the soil. This softening of soil reduces the stiffness of soil, where the system can no longer sustain the vibrations at the original frequency, resulting in a shift of the peak.

6.2.2. Amplitude-frequency variation

Fig. 5 illustrates how the amplitude of transfer functions and the corresponding resonance frequency shift for the superstructure head with respect to the smallest dynamic loading amplitude (S1). The average loading amplitude of all 4 seismic records (in m/s^2) is shown on the x-axis, while the amplitude ratio (M/M') and frequency ratio (f/f') are presented on the left and right y-axis, respectively. Here, M and f denote the transfer function amplitude and resonance frequency, whereas M' and f' denote the transfer function and resonance frequency corresponding to the smallest loading amplitude (S1).

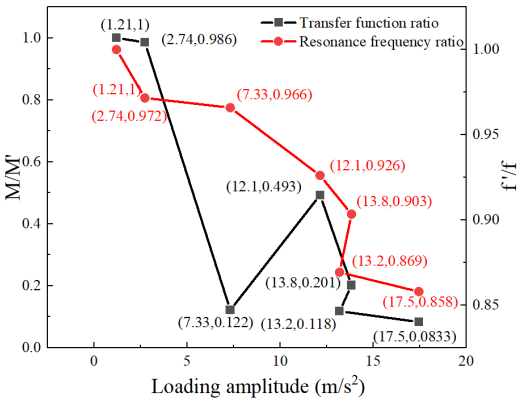

Fig. 5 Variation in transfer function amplitude and frequency of superstructure with respect to ground surface with increasing amplitude of ground motion

Both the amplitude (black line) and the resonance frequency (red line) exhibit a pronounced decline with increasing amplitude. A significant drop in both quantities is observed, particularly beyond 2.74 m/s^2, where for the amplification and frequency ratio drops to 0.0833 and 0.858 for the loading amplitude of 17.5 m/s^2. This substantial reduction indicates the onset of global and local nonlinearities in the SSI system after 2.74 m/s^2 (L1). This frequency drop is ultimately associated with the elongation of the natural period.

6.2.3. Phase difference

Fig. 6 shows the phase angle at the superstructure with respect to the ground surface, reinforcing the explanation discussed in the horizontal transfer function section. At lower amplitudes, the phase of the superstructure and the ground are the same, which is why below 15 Hz, the phase difference is zero. However, this value suddenly drops at the resonance point of the system. While the general behaviour remains similar for all amplitudes, the trend differs significantly when the system shifts from a linear to a nonlinear state.

As mentioned in the horizontal transfer function section, L1 represents the transitional amplitude. After this, the cohesion less soil softens, and a significantly larger amount of energy dissipates as compared to the lower amplitude cases. From amplitudes L2 and higher, the system partially tends to regain the prior stiffness state, but this recovery fails due to a significant loss of stiffness and contact

condition. Interestingly, this effect is prominent for L5, where the graph of the transfer function also flattens, and the phase difference follows a similar trend to other nonlinear cases.

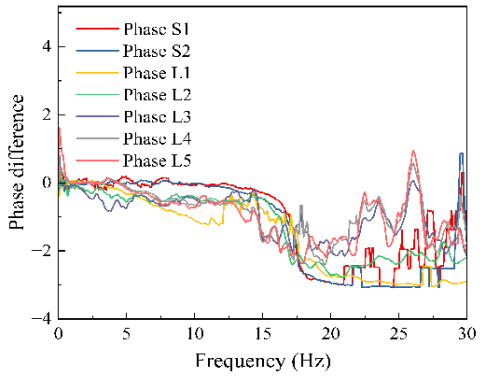

Fig. 6 Phase difference at the head of the super structure with respect to the ground surface with increasing loading amplitude

6.3. Caisson foundation head

6.3.1. Horizontal transfer function

Fig. 7 illustrates the amplitude of the horizontal transfer function for the foundation head with respect to the ground surface, subjected to earthquake records of increasing amplitude. For the caisson foundation head, the magnitude of the peak decreases with the increase in the loading amplitude. This decrease is pronounced at higher amplitudes. Similar to the superstructure case, L1 acted as a transition amplitude, as seen in Table 3. Beyond L1, the strain-dependent properties of sand become more pronounced. Hence, after yielding with the increase in strain, the sand undergoes softening, which reduces its stiffness and causes the peak shifts towards lower frequencies.

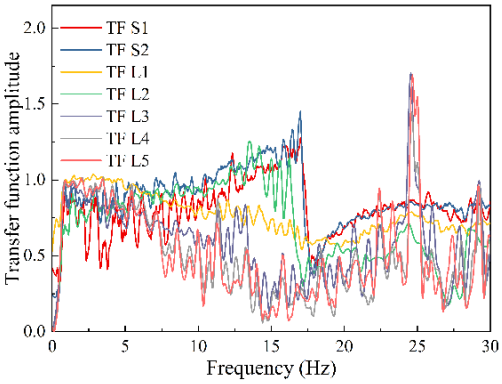

Fig. 7 Transfer function at the head of the caisson foundation with respect to the ground surface

6.3.2. Phase difference

Fig. 8 portrays the phase difference at the caisson head with respect to the ground surface. The figure demonstrates the behaviour similar to superstructure, where the response of both the caisson head and the ground surface is identical at lower frequencies. Beyond L1, the phase shifting of the caisson head has been observed simultaneously when the system shifted from linear to non-linear state. Additionally, a backward shift in the peak of the graph is observed. The loss of stiffness of the soil hinders the efficient stress transfer between the soil medium and the caisson.

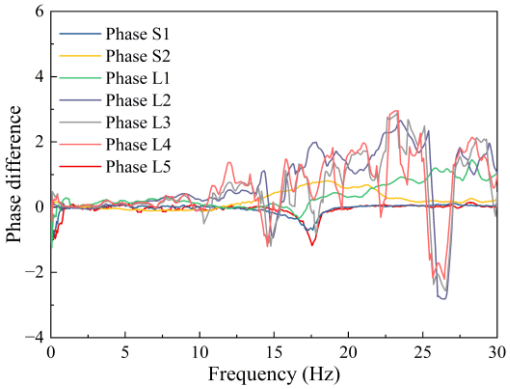

Fig. 8 Phase difference at the head of the caisson foundation with respect to the ground surface with increasing loading amplitude

6.3.3. Amplitude-frequency variation

Fig. 9 presents the variation in the transfer function amplitude and the corresponding resonance frequency shifts for the caisson head, normalized with respect to the smallest loading amplitude (S1).

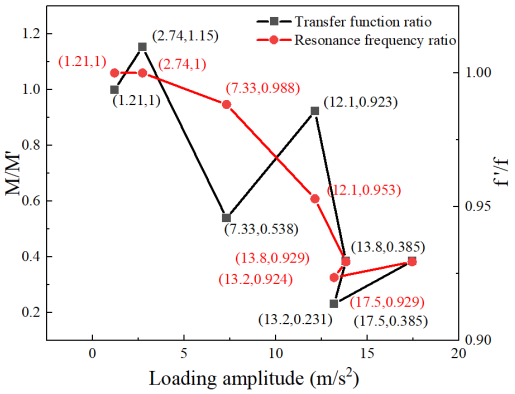

Fig. 9 Variation in transfer function amplitude and frequency of caisson head with respect to ground surface with increasing amplitude of ground motion

The x-axis shows the average loading amplitude in m/s^2, while the left and right y-axis represent the amplitude (M/M') and frequency (f/f') ratios, respectively. Both quantities decrease with an increase in amplitude, with a significant drop beyond

2.74 m/s^2, where for 17.5 m/s^2 the amplitude and frequency ratios drop to 0.385 and 0.929, respectively. Hence, a similar decreasing trend is observed for both the superstructure head and the caisson head case.

6.4. Near field pressure analysis

Fig. 11 a to d illustrates the near-field pressure response for each earthquake record at the instant when CH14 experienced peak compressive pressure. The response of the pressure transducers provides evidence of the existence of local nonlinearity. Within the linear range (at lower amplitudes), the pressure increases with the increase in loading rate, owing to the linear elastic properties of the soil material. However, as the system transits into the non-linear range at higher amplitudes, the sand exhibits inelastic behaviour. This post-yield response, localized to specific areas, leads to the degradation of the stiffness in the soil. Beyond this point, further deformation doesn't result in increased pressure, as the stress transmission mechanism diverges from that observed before local yielding. Consequently, the pressure values demonstrated variability with increasing loading amplitudes. Which can also be attributed to the generation of a gap between the sand material and the foundation, driven by interface nonlinearity. Fig. 10 shows the time histories of pressure transducers attached to the sides of the foundation close to the ground surface.

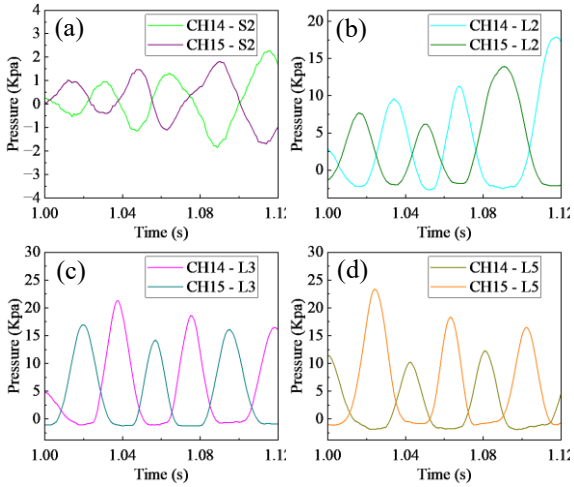

Fig. 10 Near field pressure time history for CH14/15 at a) S2, b) L2, c) L3, and d) L5

The figure indicates separation between foundation and soil, as pressure on one side drops to zero while the opposite side simultaneously reaches the peak at higher amplitudes. For instance, at S2, the pressure response is sinusoidal, indicating no separation at lower amplitude. However, at higher amplitudes, the pressure transducers recorded only positive values, indicating separation between the foundation and the soil.

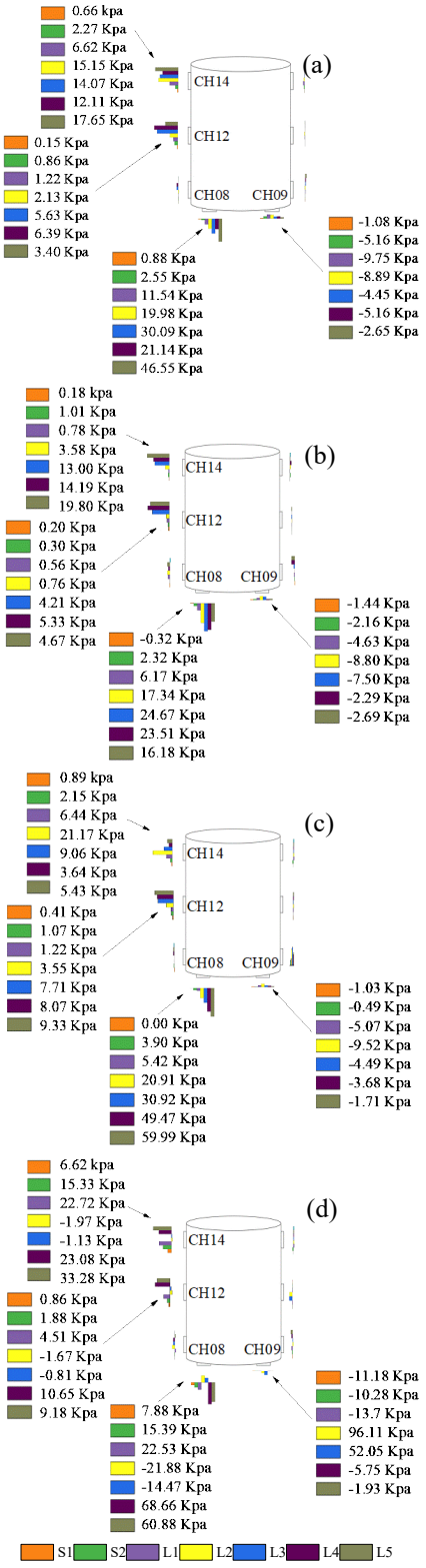

Fig. 11 Near field pressure response for a) El-Centro, b) Kobe, c) Ojiya, and d) White noise earthquake records

7. CONCLUSIONS

By focusing on critical systems behaviours and conditions that might result in significant damage, this study presented the experimental results on the nonlinear inertial effects in the soil-caisson-superstructure system against increasing amplitude of different earthquake records. It explored the effects of rising amplitude on the amplification ratio and the mechanism of soil-structure interaction, including near-field pressure response for local nonlinearities and mean shear strain for both local and global nonlinearities.The resonance peaks were obtained for the amplification ratio graph with the increase in the amplitude. The findings reveal that these resonance peaks in the horizontal transfer function (for the superstructure top and the caisson head) flatten as the loading amplitude increases. This is attributed to the increased energy dissipation in soil, leading to high damping because of global nonlinearities in the soil. In global nonlinear behaviour, when the stiffness of the soil decreases, the dissipation of energy increases, leading to an increase in damping. Owing to this, the peak of the amplification ratio reduces progressively as the amplitude increases, while the natural time period elongates, reflecting the degradation in the stiffness of the soil. The observation is further supported by the mean shear strain, which shows higher values at higher loading amplitudes. In addition to global nonlinearity, the near-field pressure response justifies the observation of local nonlinearity in the system. The pressure values increase gradually at lower amplitudes, whereas they become staggered at higher amplitudes, reflecting the presence of some local interface nonlinearities. The prediction of the separation between the foundation and the soil is also validated from the time history of pressure responses. The loss of contact between the foundation and the structure is observed at higher amplitudes, significantly compromising the transmission of inertial forces.

These findings highlight the need to account for global and local nonlinearities in structural design. providing critical insights for developing resilient and safer infrastructure under extreme seismic conditions.

Future work should incorporate harmonic excitation tests to closely investigate the dynamic behavior in the vicinity of the predominant frequencies observed in the experiments. Additionally, In addition, finite element analysis should be employed to assess the reproducibility of the experimental results and to elucidate the underlying mechanisms.

8. ACKNOWLEDGEMENTS

This work was supported by KAKENHI Grant-in-Aid for Scientific Research (B) 21H01414 from the Japan Society for the Promotion of Science.

9. REFERENCES

[1] Nagai H., Evaluation of dynamic interaction factor of rectangular piled raft foundation for horizontal and rotational motio, International Journal of GEOMATE, Vol. 20, Issue 77, 2021, pp. 107-115.

[2] Wu Y., Peng T., and Ahmad S., 1-g Shaking Table Test Study on the Influence of Soil–Caisson Dynamic Interaction (SCDI) on the Caisson Foundation Motion, Applied Sciences, Vol. 14, Issue 19, 2024. https://doi.org/10.3390/app14198942.

[3] Matsui T., Foundation damage of structures in Kobe and remediation, Proceedings of the 4th International Conference on Case Histories in Geotechnical Engineering, 1998.

[4] Goit C.S., Honma S., Saitoh M., and Giri P., Effects of Soil Nonlinearity on the Seismic Behavior of Pile Foundations Reinforced with Micropiles, International Journal of Geomechanics, Vol. 24, Issue 10, 2024. https://doi.org/10.1061/IJGNAI.GMENG-9600.

[5] Gaudio D., and Rampello S., Equivalent seismic coefficients for caisson foundations supporting bridge piers, Soil Dynamics and Earthquake Engineering, Vol. 129, 2020. https://doi.org/10.1016/j.soildyn.2019.105955.

[6] Erdogan D., Mahmudi M., and Erözkan E., Effect of Inertia of Superstructure on Seismic Response of Shallow Foundations, 8th International Geotechnical Symposium, 2019.

[7] Ullah M.S., Kajiwara K., Goit C.S., and Saitoh M., Frequency and intensity dependent dynamic responses of soil-steel pipe sheet pile (SPSP) foundation-superstructure system, Soil Dynamics and Earthquake Engineering, Vol. 25, 2019, pp. 1-8.

[8] Goit C.S., Saitoh M., Kawakami H., and Nishiyama S., Experimental studies on non-linear response of soil-pile-structure systems subjected to strong ground motion, In Proceedings of the 14th World Conference on Earthquake Engineering, 2008.

[9] Ullah M.S., Yamamoto H., Goit C.S., and Saitoh M., On the verification of superposition method of kinematic interaction and inertial interaction in dynamic response analysis of soil-pile-structure systems, Soil Dynamics and Earthquake Engineering, Vol. 113, 2018, pp. 522-33. https://doi.org/10.1016/j.soildyn.2018.06.023.

[10] Veletsos A.S., and Meek J.W., Dynamic behaviour of building-foundation systems, Earthquake Engineering & Structural Dynamics, Vol. 3, Issue 2, 1974, pp. 121-38. https://doi.org/10.1002/eqe.4290030203.

[11] Bielak J., Dynamic behaviour of structures with embedded foundations. Earthquake Engineering & Structural Dynamics, Vol. 3, Issue 3, 1974, pp. 259-74. https://doi.org/10.1002/eqe.4290030305.

[12] Kagawa T., On the similitude in model vibration tests of earth-structures, In Proceedings of the Japan Society of Civil Engineers, Issue 275, 1978, pp. 69-77. https://doi.org/10.2208/jscej1969.1978.275_69.

[13] Zafar U., Goit C.S., Saitoh M., and Fukuda R., Vertical impedance functions of pile groups under low-to-high loading amplitudes: numerical simulations and experimental validation, Earthquake Engineering and Engineering Vibration, Vol. 22, Issue 3, 2023, pp. 647-66. https://doi.org/10.1007/s11803-023-2183-y.

[14] Shrestha N.R., Saitoh M., Saha A.K., and Goit C.S., Frequency-and intensity-dependent impedance functions of laterally loaded single piles in cohesionless soil, Soils and Foundations, Vol. 61, Issue 1, 2021, pp. 129-43. https://doi.org/10.1016/j.sandf.2020.11.004.

[15] Zafar U., Goit C.S., and Saitoh M., Experimental and numerical investigations on vertical dynamic pile-to-pile interactions considering soil and interface nonlinearities, Bulletin of Earthquake Engineering, Vol. 20, Issue 7, 2022, pp. 3117-42. https://doi.org/10.1007/s10518-021-01186-x.

[16] Rahman M., Soma I., Goit C.S., and Saitoh M., Seismic Performance of Pile Foundations Reinforced with Micropiles, InEast Asia-Pacific Conference on Structural Engineering and Construction, 2024, pp. 530-537. doi: 10.1007/978-981-96-8464-9_67.